XLI CILAMCE
XLI Ibero-Latin American Congress on Computational Methods in Engineering
16-19 November, 2020 FOZ DO IGUAÇU PARANÁ - BRAZIL

# A Boundary Element Coupling formulation for three-dimensional reinforced domains

Antonio R. Neto[1], Edson D. Leonel[1]

[1]*Department of Structural Engineering, São Carlos School of Engineering, University of São Paulo*
*Av. Trabalhador SaoCarlense,400 , CEP 13566-590, São Carlos-SP, Brazil*
*anotonio.rodrigues.neto@usp.br, edleonel@sc.usp.br*

**Abstract.** This study presents a numerical coupling formulation for the mechanical modelling of reinforced three-dimensional (3D) structural systems. This formulation is based on the Boundary Element Method (BEM) for the mechanical analysis of 3D domains with Lagrangian approximation. In this coupling, the material matrix (solid 3D domain) is represented by the usual 3D BEM formulation with Kelvin's fundamental solutions for isotropic linear-elastic materials. Numerical integration and singularity subtraction are applied herein. A one-dimensional approach of the BEM (1DBEM) represents the embedded fibre-reinforcements, which enforce axial mechanical solicitation. The 1DBEM is based on the axial fundamental solution for elastic 1D domains, which can be easily found in the literature. The interaction between the matrix and reinforcements is described by an adherence force over the reinforcements' line, which is interpolated by high-order Lagrangian functions. One considers no relative displacements (perfect bonding). The adherence force is accounted as a body force into the 3D BEM formulation. These aspects characterise the proposed 1DBEM/BEM coupling as an alternative to the usual FEM/BEM technique, which has been widely applied in the literature. The authors have previously demonstrated in Rodrigues Neto and Leonel [1] that the 1DBEM/BEM coupling exhibits superior results when compared against the usual FEM/BEM approach in 2D applications. This work presents the extension of this formulation for 3D analyses. The proposed modelling is applied herein in the mechanical analysis of complex 3D applications. The achieved results are compared against experimental responses available in the literature. The proposed formulation led to accurate and stable results.

**Keywords:** Coupled BEM formulation, Reinforced materials, 3D BEM, FEM/BEM

## 1 Introduction

The coupling of reinforced materials and components enables the design of efficient structural systems, in which high stiffness and low weight are achieved. These structural systems compositions have been progressively increased in several designs recently. With that, its accurate mechanical modelling becomes indispensable for numerous engineering areas. In this regard, the coupling of dissimilar numerical methods is an interesting approach, in which the FEM/BEM (Finite Element Method/Boundary Element Method) coupling proposed by Zienkiewicz et al. [2] stands out. The BEM represents the solid matrix and 1D finite elements model the reinforcing fibres in this coupling technique. Rodrigues Neto and Leonel [1] proposed an alternative coupling formulation based only in BEM approaches, named 1DBEM/BEM, for 2D analyses. This scheme led to accurate and superior performance in comparison with classical numerical schemes.

This study presents extension of the 1DBEM/BEM coupling formulation for 3D analyses. 3D BEM singular formulation is applied herein to describe the solid matrix mechanical behaviour, accounting for Lagrangian approximation. Whereas 1DBEM elements in space model the embedded fibres. A particular integration scheme for the reinforcement elements is described, in order to make the kinematic assumptions from 3D BEM and 1DBEM compatible. A numerical application demonstrates the accuracy and robustness of the proposed formulation. Random fibres are numerically modelled, considering experimental reference results available.

## 2 1DBEM/BEM coupling formulation

### 2.1 3D BEM singular formulation

The BEM displacements integral equation represents the solid ($\Omega$) mechanical behaviour. This equation can be obtained through the weighted residual technique, as presented by Brebbia [3], and it is written as follows:

$$c_{ij}(\mathbf{x}^s)u_j(\mathbf{x}^s) + \int_\Gamma T^*_{ij}u_j(\mathbf{x}^f)d\Gamma = \int_\Gamma U^*_{ij}p_j(\mathbf{x}^f)d\Gamma + \int_\Omega U^*_{ki}b_i d\Omega \tag{1}$$

in which $u_i$ and $p_i$ represent displacements and tractions at the boundary, respectively. $\Gamma$ is the boundary of $\Omega$. $c_{ij}$ is the free term, which is equal to the Kronecker delta ($\delta_{ij}$) for internal points and $0.5\delta_{ij}$ for points at smooth boundaries. $U^*_{ij}$ and $T^*_{ij}$ are the Kelvin's fundamental solutions for displacements and tractions, respectively, which can be found in Brebbia and Dominguez [4].

The BEM solves Eq. 1 in approximate form. Then, the geometry and mechanical fields are approximated by Lagrangian isoparametric elements positioned at the boundary ($\Gamma$). Quadrilateral linear elements (4 nodes) are implemented in this work. Besides, non-smooth geometries and discontinuous boundary conditions can be handled through discontinuous and semi-continuous boundary elements. Equation. 1 must be evaluated for all collocation points (source points) to represent the solid's mechanical behaviour. Because of the singular nature of the fundamental solutions, singularity subtraction technique is applied herein, as presented in Guiggiani et al. [5]. Otherwise, the regular kernels are numerically integrated by Gauss-Legendre scheme. Hence, Eq. 1 can be algebraically written as follows:

$$\mathbf{Hu} = \mathbf{Gp} + \int_\Omega U^*_{ki}b_i d\Omega \tag{2}$$

where the matrices $\mathbf{H}$ and $\mathbf{G}$ contain, respectively, the integration of kernels $T^*_{ij}$ and $U^*_{ij}$ along $\Gamma$. The domain term has not been treated so far, thus it cannot be written in a algebraic form. This term will be numerically treated in the coupling formulation section.

Equation 1 can also be used to represent internal points' displacements. This expression is algebraically written as follows:

$$\mathbf{u_i} + \mathbf{Hu} = \mathbf{Gp} + \int_\Omega U^*_{ki}b_i d\Omega \tag{3}$$

where $u_i$ is the vector of displacements of the internal point $i$.

### 2.2 1DBEM in space: reinforcements modelling

The 1DBEM displacements integral equation can also be obtained through the weighted residual technique applied for 1D domains ($\bar{x}$), as described in Rodrigues Neto and Leonel [1], and it is written as follows:

$$u_i - N^*_{i1}u_1 + N^*_{in}u_n = -u^*_{i1}N_1 + u^*_{in}N_n + \int_0^L \phi_j(\bar{x})\, u^*_{i\bar{x}}\, d\bar{x}\; p_j \tag{4}$$

in which subscripts 1 and $n$ represent the 1D domain endpoints. $u_i$ and $N_i$ are, respectively, the axial displacement and internal force at the $i$ point. $\phi_j$ are the Lagrangian functions used for the distribuited load approximation over the domain $\bar{x}$, using its nodal values $p_i$. $u^*_{ij}$ and $N^*_{ij}$ are the fundamental solutions for axial displacements and internal forces, respectively, which can be found in Banerjee and Butterfield [6], Antes [7].

The integral formulation (Eq. 4) requires the discretisation of the structural boundaries into parametric elements. One notices that the boundary is composed only of the 1D element endpoints, i.e., $i = 1$ and $i = n$. Any other value for $i$ leads to an internal point equation. However, internal points are accounted in the 1DBEM algebraic system, to improve the accuracy of the distributed load representation. Hence, the 1DBEM formulation enables high-order isoparametric elements. Thus, after applying the element's approximations, Eq. 4 can be algebraically written as follows:

$$\bar{\mathbf{H}}\mathbf{u} = \bar{\mathbf{G}}\mathbf{n} + \bar{\bar{\mathbf{G}}}\mathbf{p} \tag{5}$$

where $\bar{\mathbf{H}}$ and $\bar{\mathbf{G}}$ contain the values of the fundamental solutions $N^*_{sf}$ and $u^*_{sf}$, respectively, applied in the boundary points. $\mathbf{u}$, $\mathbf{p}$ and $\mathbf{n}$ vectors contain, respectively, the nodal values of axial displacement, nodal values of distributed force and concentrated loads. This expression is so far valid for the local coordinate system. The following global expression can be written by applying axial rotation, as described in Kassimali [8], and considering $\mathbf{n} = \mathbf{0}$:

$$\mathbf{K_F u_F} = \mathbf{G_F p_F} \tag{6}$$

in which $\mathbf{u_F}$ and $\mathbf{p_F}$ vectors contain the values of $\mathbf{u}$ and $\mathbf{p}$ in the global coordinate system.

### 2.3 Algebraic representation of the coupling formulation

Consider the reinforcements completely embedded into the solid $\Omega$ and positioned along the line $\bar{\Gamma}$, as illustrated in Fig. 1(a). The coupling scheme accounts for the mechanical interaction among reinforcements and domain, which is represented by the adherence force as illustrated in Fig. 1(b).

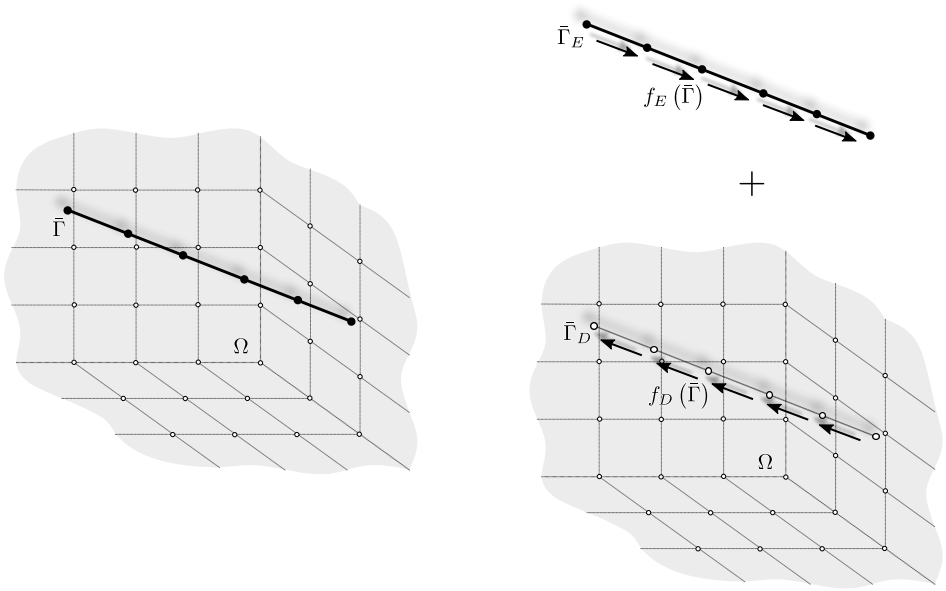


(a) (b)

Figure 1. Scheme of domain/reinforcement coupling technique.

The adherence force is modelled as one-dimensional distributed load along the reinforcement's line $\bar{\Gamma}$. However, one-dimensional loads applied in a three dimensional domain lead to divergent singular values in the fundamental solutions, i.e., which cannot be regularised. Thus, a matching approximation is required, which is similar to the "special element" proposed for FEM/BEM couplings in Coda et al. [9]. The adherence force in $\Omega$ is assumed to be applied over a two-dimensional surface, which represents the external surface area of the reinforcements. A cylindrical shell of radius $R_F$ is adopted herein. Considering the reinforcements as thin elements, i.e., with a length higher than $R_F$, one can writes the following simplification:

$$\mathbf{p_D} = 2\pi R_F \mathbf{Q_i} \tag{7}$$

where $\mathbf{Q_i}$ is the value of the distribuited force over the cylindrical shell, assumed as constant along the angular direction $\theta$.

Thus, the integration of the adherence force over the reinforcements elements can be accounted in the domain term of Eq. 1 and numerically evaluated as follows:

$$\begin{aligned}&\int_{\bar{\Gamma}} U^*_{ij}(\mathbf{p_D})_j d\Gamma = \\ &\sum_{g_1=1}^{np_1}\left[\sum_{g_2=1}^{np_2}\left[U_{ij}\left(\mathbf{x}^f(\xi_{g_1},\xi_{g_2}),\mathbf{x}^s\right)|\mathbf{jac_2}(\xi_{g_2})|\,\omega_{g_2}\right]|\mathbf{jac_1}(\xi_{g_1})|\,\omega_{g_1}\phi_m(\xi_{g_1})\right]\frac{(\mathbf{p_D})_j}{2\pi R_F}\end{aligned} \tag{8}$$

where $g_1$ and $g_2$ represent the numerical integrations used for the axial coordinate ($\bar{x}$) and the angular coordinate ($\theta$), respectively. $\xi_i$, $\omega_{g_i}$ and $np_i$ are the dimensionless coordinates, weight values and total number of integration points of the numerical integration $i$, respectively. The modulus of the Jacobian vector ($\mathbf{jac}_i(\xi_{g_i})$) of each integration is determined as follows:

$$|\mathbf{jac}_1(\xi_{g_1})| = \sqrt{\left(x^b_{1,\xi}(\xi_{g_1})\right)^2 + \left(x^b_{2,\xi}(\xi_{g_1})\right)^2 + \left(x^b_{3,\xi}(\xi_{g_1})\right)^2} \tag{9a}$$

$$|\mathbf{jac_2}(\xi_{g_2})| = \pi R_F \tag{9b}$$

where $x^b_i$ are the coordinates of the $\mathbf{x}^b(\xi_{g_2})$ point, which is the projection of the field point $\mathbf{x}^f$ along the axial axis $\bar{x}$. This axis is coincident with the reinforcements line $\bar{\Gamma}$. The numerical integration mapping over the axial direction defines the position of the $\mathbf{x}^b(\xi_{g_2})$ point. Likewise, the numerical integration mapping over the angular direction defines the value of $\theta(\xi_{g_2})$. Thus, the field point is defined as a function of the dimensionless coordinates as follows:

$$\mathbf{x}^f = \mathbf{x}^b(\xi_{g_1}) + \frac{R_F}{\sqrt{\cos^2(\alpha_1) + \cos^2(\alpha_2)}} \begin{Bmatrix} -\cos(\alpha_2)\cos\left(\theta(\xi_{g_2})\right) - \cos(\alpha_1)\cos(\alpha_3)\sin\left(\theta(\xi_{g_2})\right) \\ \cos(\alpha_1)\cos\left(\theta(\xi_{g_2})\right) - \cos(\alpha_2)\cos(\alpha_3)\sin\left(\theta(\xi_{g_2})\right) \\ \left[\cos^2(\alpha_1) + \cos^2(\alpha_2)\right]\sin\left(\theta(\xi_{g_2})\right) \end{Bmatrix} \tag{10}$$

in which $\alpha_i$ are the coordinates between the axis $\bar{x}$ and the global axis $x_i$ at the point $\mathbf{x}^b$.

Figure 2 illustrates the integration over a reinforcement element considering a source point positioned at $\bar{\Gamma}$, considering $np_2 = 4$ and a fixed coordinate $\xi_{g_1}$.

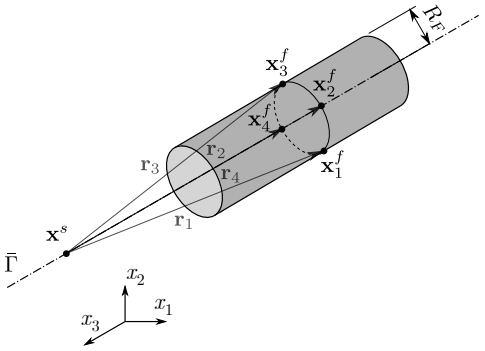


Figure 2. Integration scheme over a reinforcement element, considering 4 integration points over the angular coordinate and a fixed axial coordinate.

Therefore, the adherence force can be properly accounted as a body force into the BEM formulation through Eq. 8. Hence, the BEM integral equation for boundary points (Eq. 2) can be rewritten as follows:

$$\mathbf{H_{CC}u_C} = \mathbf{G_{CC}p_C} + \mathbf{G_{CF}p_D} \tag{11}$$

where the term $\mathbf{G_{CF}p_D}$ is the particular form of the domain term obtained by applying Eq. 8. The subscripts $\mathbf{C}$ and $\mathbf{F}$ indicate boundary and fibre, respectively. The subscript $\mathbf{D}$ indicates the internal point of $\Omega$ coincident with a fibre point. In the above equation, a matrix $\mathbf{H_{XY}}$ or $\mathbf{G_{XY}}$ result from source point at $\mathbf{X}$ and field point at $\mathbf{Y}$.

The BEM integral equation for internal points (Eq. 3) can also be rewritten herein. This equation must be applied for internal points coincident with the reinforcements nodes, i.e., $\mathbf{u_i} = \mathbf{u_D}$. Thus:

$$\mathbf{u_D} = \mathbf{G_{FC}p_C} - \mathbf{H_{FC}u_C} + \mathbf{G_{FF}p_D} \tag{12}$$

The proposed model assumes perfect bond conditions among reinforcements and domain. Then, the compatibility of displacements and equilibrium of forces are enforced among reinforcements and domain as follows:

$$\mathbf{u_F} = \mathbf{u_D} \qquad \text{and} \qquad \mathbf{p_F} = \mathbf{p_D} \tag{13}$$

The resulting algebraic system of equations is then obtained by coupling Eq. 11, Eq. 12 and Eq. 5. In addition, the application of the compatibility relations from Eq. 13 leads to:

$$\begin{bmatrix} \mathbf{H_{CC}} & \mathbf{0} & -\mathbf{G_{CF}} \\ \mathbf{H_{FC}} & \mathbf{I} & -\mathbf{G_{FF}} \\ \mathbf{0} & \mathbf{K_F} & \mathbf{G_F} \end{bmatrix} \begin{Bmatrix} \mathbf{u_C} \\ \mathbf{u_D} \\ \mathbf{p_D} \end{Bmatrix} = \begin{bmatrix} \mathbf{G_{CC}} \\ \mathbf{G_{FC}} \\ \mathbf{0} \end{bmatrix} \{\mathbf{p_C}\} \tag{14}$$

where $\mathbf{I}$ is the identity matrix. The last equation is solved by enforcing the boundary conditions, as usual in BEM. The final algebraic system is as follows:

$$\begin{bmatrix} \mathbf{A_{CC}} & \mathbf{0} & -\mathbf{G_{CF}} \\ \mathbf{B_{FC}} & \mathbf{I} & -\mathbf{G_{FF}} \\ \mathbf{0} & \mathbf{K_F} & \mathbf{G_F} \end{bmatrix} \begin{Bmatrix} \mathbf{x_C} \\ \mathbf{u_D} \\ \mathbf{p_D} \end{Bmatrix} = \begin{bmatrix} \bar{\mathbf{A}}_{\mathbf{CC}} \\ \bar{\mathbf{B}}_{\mathbf{FC}} \\ \mathbf{0} \end{bmatrix} \{\tilde{\mathbf{p}}_{\mathbf{C}}\} \tag{15}$$

in which the matrices $\mathbf{A_{CC}}$, $\mathbf{B_{FC}}$, $\bar{\mathbf{A}}_{\mathbf{CC}}$ and $\bar{\mathbf{B}}_{\mathbf{FC}}$ result from the columns change procedure. $\tilde{\mathbf{p}}_{\mathbf{C}}$ and $\mathbf{x_C}$ are the known and unknown values at the boundary, respectively.

## 3 Numerical application

The numerical application handles the mechanical analysis of a concrete specimen reinforced by short fibres, which are pseudo-randomly distributed within the concrete. The stiffening effect of different fibre volume is measured through the equivalent longitudinal elastic modulus ($E_{ef}$). An uniaxial stress scenario is simulated for the experimental compression test, as illustrated in Fig. 3(a). This numerical model consists of a 20 mm diameter cylinder with 20 mm length. The following physical properties are considered: Young's modulus $E_M = 39.6$ GPa and Poisson ratio $\nu = 0.2$ for the concrete. The fibres have length of 13 mm, radius equals 0.1 mm and Young's modulus $E_f = 220$ GPa. The experimental test scheme is illustrated in Fig. 3(b) and Krahl et al. [10] presents experimental results, which are used herein as reference.

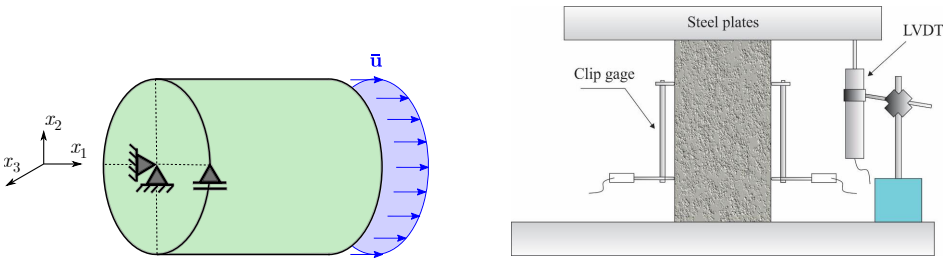


(a) (b)

Figure 3. Numerical application of the elastic coupling: numerical model (a) an experimental scheme (b) for an uniaxial compression test. Krahl et al. [11], adapted.

The equivalent longitudinal elastic modulus can be determined as follows:

$$E_{ef} = \frac{L}{\bar{u}_1 \pi r^2} \int_{\Gamma_s} t_1 \left(\Gamma\right) d\Gamma \tag{16}$$

where $L$ is the cylinder, $r$ is the cylinder radius (in the plane $x_2\, x_3$). $\Gamma_s$ is the cylinder face where $\bar{\mathbf{u}}$ is applied and $t_1 \left(\Gamma\right)$ are the traction results at the boundary.

The boundary mesh is composed of 4250 linear quadrilateral elements and 4442 collocation points. Figure 4 illustrates this mesh. Each short fibre is discretised into 5 quadratic 1DBEM elements. Previous analyses have shown mesh convergence regarding displacements over the boundary and $E_{ef}$ results.

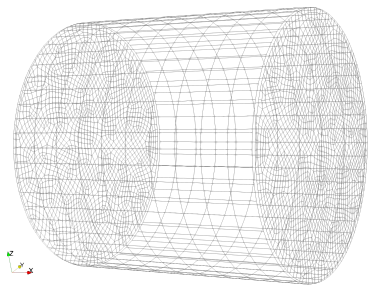

Figure 4. Boundary mesh utilised for the cylinder representation.

Steel-fibre reinforced concrete specimens were used in the experimental results of Krahl et al. [10]. Three different fibre's content in volume were analysed: 0%, 1% and 2%. One disregards the physical nonlinearities because the linear-elastic limit in compression was respected.

Four different fibre's pseudo-random scenarios are assumed for the numerical analysis, which aims the accurate representation of the fibres spacial position:

- "$\text{BEM}_{\text{rand}}$" assumes fibre position and fibre inclination governed by uniform statistical distribution. This scenario leads to random distributed fibres;
- "$\text{BEM}_{\text{alig}}$" assumes fibre position governed by uniform statistical distribution and inclination aligned with the $x_1$ axis;
- "$\text{BEM}_{\text{transv}}$" assumes fibre position governed by uniform statistical distribution and inclination aligned with $x_2$ axis;
- "$\text{BEM}_{\text{normal}}$" assumes fibre position governed by uniform statistical distribution and inclination governed by Gaussian bi-variate statistical distribution with standard deviations equal to 0.23 rad. This scenario leads to pseudo-random fibres with a preferential direction.

The standard deviations value of the Fourth scenario were previously calibrated to best match the experimental results. Figure 5 illustrates the results obtained with the four above-mentioned scenarios in addition to the experimental responses. Such comparison has been performed through the relation between the equivalent elastic modulus ($E_{ef}$) and the matrix Young's modulus ($E_M$). All results are presented as the tendency line (from a linear regression) of the multiple values obtained for each point, besides the actual results of some scenarios ("val."). Figure 5(a) considers the random numerical scenarios ($\text{BEM}_{\text{rand}}$, $\text{BEM}_{\text{alig}}$ and $\text{BEM}_{\text{transv}}$), in addition to the maximum ("max") and minimum ("min") values of the experimental results. Figure 5(b) illustrates the calibrated numerical scenario $\text{BEM}_{\text{normal}}$.

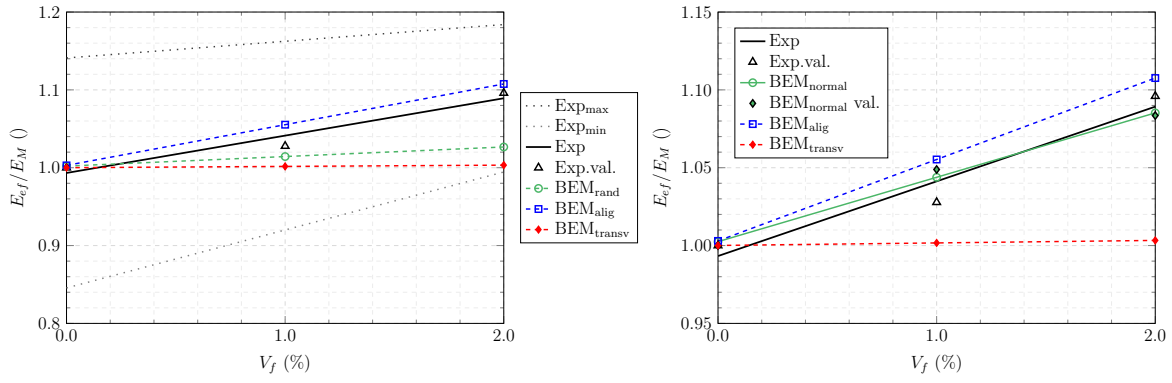


(a) (b)

Figure 5. Stiffness variation as a function of the fibre volume using different distributions of fibres in the numerical model: random distributions (a) and calibrated distribution (b)

Figure 5 demonstrates the good agreement among the numerical responses and the reference. Figure 5(a) suggests that the experimental mean responses are between the $\text{BEM}_{\text{rand}}$ and $\text{BEM}_{\text{alig}}$ results. Besides, 5(b) illustrates that the $\text{BEM}_{\text{normal}}$ scenario was able to accurately match the reference. Thus, a possible uncertainty about the fibres randomness are observed in the experimental results, which have been often recognised in the literature as mentioned by Gettu et al. [12], Yoo et al. [13].

Figure 6 illustrates the displacements along $x_1$ direction over the reinforcement's mesh. $\text{BEM}_{\text{normal}}$ model with $V_f = 1\%$ is illustrated in Fig. 6(a) and $\text{BEM}_{\text{rand}}$ with $V_f = 2\%$, in Fig. 6(b). A tension scenario ($\bar{\mathbf{u}}_{\mathbf{D}} = 1$ mm) was considered herein. The pseudo-random spacial fibres position distribution $\text{BEM}_{\text{normal}}$ is observed in Fig. 6(a). Furthermore, all displacements behaviour in both figures are within the expected range, due to the prescribed displacement applied.

## 4 Conclusions

The 1DBEM/BEM coupled formulation for the mechanical analysis of 3D reinforced structures and materials was successfully presented in this study. The numerical application demonstrate its robustness and accuracy in modelling complex 3D engineering problems, such as the random-distribuited short fibres. The obtained results were coherent and in agreement with the experimental reference. The 3D aspect of the presented formulation is highlighted herein to properly represent any fibres distribution and inclination in space. The efficiency of the formulation was also illustrated, regarding the reduced number of degrees of freedom to discretise both specimen boundary and short fibres. Therefore, the proposed formulation is robust, stable and has large potential for solving complex real-life structural problems.

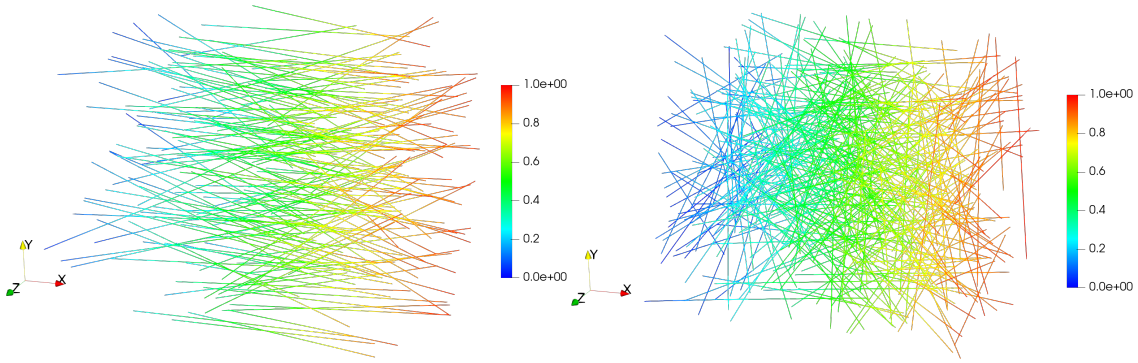


(a) (b)

Figure 6. Displacement in $x_1$ direction over the reinforcements using: normal distributed fibres $\text{BEM}_{\text{normal}}$ in (a) and random distributed fibres $\text{BEM}_{\text{rand}}$ in (b)

**Acknowledgements.** Sponsorship of this research project by the São Paulo State Foundation for Research (FAPESP), project number 2018/20253-4, is greatly appreciated.

**Authorship statement.** The authors hereby confirm that they are the sole liable persons responsible for the authorship of this work, and that all material that has been herein included as part of the present paper is either the property (and authorship) of the authors, or has the permission of the owners to be included here.

## References

[1] Rodrigues Neto, A. & Leonel, E. D., 2019. The mechanical modelling of nonhomogeneous reinforced structural systems by a coupled BEM formulation. *Engineering Analysis with Boundary Elements*, vol. 109, pp. 1 – 18.

[2] Zienkiewicz, O., Kelly, D., & Bettess, P., 1977. The coupling of the finite element method and boundary solution procedures. *International journal for numerical methods in engineering*, vol. 11, n. 2, pp. 355–375.

[3] Brebbia, C. A., 1978. Weighted residual classification of approximate methods. *Applied Mathematical Modelling*, vol. 2, n. 3, pp. 160 – 164.

[4] Brebbia, C. & Dominguez, J., 1994. *Boundary Elements: An Introductory Course*. Sydney Grammar School Press.

[5] Guiggiani, M., Krishnasamy, G., Rudolphi, T. J., & Rizzo, F. J., 1992. A General Algorithm for the Numerical Solution of Hypersingular Boundary Integral Equations. *Journal of Applied Mechanics*, vol. 59, n. 3, pp. 604–614.

[6] Banerjee, P. K. & Butterfield, R., 1981. *Boundary element methods in engineering science*, volume 17. McGraw-Hill, London.

[7] Antes, H., 2003. Fundamental solution and integral equations for timoshenko beams. *Computers & structures*, vol. 81, n. 6, pp. 383–396.

[8] Kassimali, A., 2012. *Matrix Analysis of Structures*. Cengage Learning, Stamford, 2 edition.

[9] Coda, H. B., Venturini, W. S., & Aliabadi, M. H., 1999. A general 3D BEM/FEM coupling applied to elastodynamic continua/frame structures interaction analysis. *International Journal for Numerical Methods in Engineering*, vol. 46, n. 5, pp. 695–712.

[10] Krahl, P. A., Carrazedo, R., & El Debs, M. K., 2018. Mechanical damage evolution in UHPFRC: experimental and numerical investigation. *Engineering Structures*, vol. 170, pp. 63–77.

[11] Krahl, P. A., Gidrão, G. d. M. S., & Carrazedo, R., 2019. Cyclic behavior of UHPFRC under compression. *Cement and Concrete Composites*, vol. 104, pp. 103363.

[12] Gettu, R., Gardner, D. R., Saldivar, H., & Barragán, B., 2005. Study of the distribution and orientation of fibers in sfrc specimens. *Materials and Structures*, vol. 38, n. 1, pp. 31–37.

[13] Yoo, D.-Y., Banthia, N., Kang, S.-T., & Yoon, Y.-S., 2016. Effect of fiber orientation on the rate-dependent flexural behavior of ultra-high-performance fiber-reinforced concrete. *Composite Structures*, vol. 157, pp. 62–70.